iScience

CellPress
OPEN ACCESS

Perspective

15 years of spin-echo spectroscopy at SNS-NSE: Looking back and looking forward

Piotr A. Zolnierczuk,[1,*] Laura-R. Stingaciu,[1] Olaf Holderer,[2] and Michael Monkenbusch[3]
[1]Neutron Sciences Directorate, Oak Ridge National Laboratory (ORNL), 1 Bethel Valley Road, Oak Ridge, TN 37831, USA
[2]Jülich Centre for Neutron Sciences at Heinz Maier-Leibnitz Zentrum (JCNS at MLZ), Forschungszentrum Jülich GmbH, Lichtenbergstr. 1, 85747 Garching, Germany
[3]Jülich Centre for Neutron Sciences (JCNS-1), Forschungszentrum Jülich GmbH, Leo-Brandt-Str, 52425 Jülich, Germany
*Correspondence: zolnierczukp@ornl.gov
https://doi.org/10.1016/j.isci.2025.113017

SUMMARY

High-resolution neutron spin echo (NSE) spectroscopy offers unique insights into the mobility of molecular (sub)structures excited by thermal fluctuations (i.e., Brownian motion) of "soft matter" as polymers in solution and in the melt, in biological matter (e.g., protein motions), membranes, and glasses. The ability to tag substructures using H, D contrast variation to resolve the relevant timescales of dynamics on selected molecular items in liquids, soft matter, and melts is a significant advantage of NSE. Also slow magnetic fluctuations on molecular length scales in the range of nanoseconds, e.g., in spin glasses or topological spin structures, can be accessed. This paper reviews the highlights and peculiarities of the SNS-NSE, based at the pulsed neutron source SNS, during its first 1.5 decades of operation. An outlook and perspectives of research in the domain of high-resolution spectroscopy is given.

INTRODUCTION

High resolution neutron spin echo (NSE) spectroscopy is the highest energy resolution technique involving cold neutrons.[1] It was invented by Ferenc Mezei in 1972[2,3] and first realized at the ILL with the IN11 instrument.[3] This powerful technique allows us to delve into the fascinating world of thermally driven fluctuations on nanometer length scales and picosecond to 100 s of nanosecond timescales. Thermally driven fluctuations play a crucial role in various complex systems, including biological membranes, protein function, polymer melts, and paramagnetic or magnetic fluctuations. In biological membranes for example, membrane fusion and transport through the membrane relies on its elasticity which can be probed by measuring the thermal fluctuations with NSE.[4] Protein function is not only related to its structure but also to thermally driven domain motion.[5] Diffusion and protein mobility also plays a crucial role in oxygen uptake and transport by hemoglobin.[6] But also in the area of hard condensed matter, slow magnetic fluctuations play an important role, for example for spin glasses or skyrmions[7,8] The SNS-NSE spectrometer[9,10] (Figure 1) located at the BL-15 of the Spallation Neutron Source (SNS), Oak Ridge National Laboratory is currently the only "classic" NSE spectrometer installed at a pulsed neutron source. It is also the first successful, user serving, high resolution NSE instrument to employ superconducting coils.

The development of the NSE spectroscopy has continuously evolved from its very start with the construction of the IN11 at ILL to the SNS-NSE with superconducting coils and beyond (such as optimized main solenoid field shapes for the most recent developments, e.g., Pasini et al.[11]), spanning a half of a century from the 1970s to the present. Early on the idea for an NSE instrument at a pulsed source was put forward[12] and a proof of concept utilizing a set of choppers at IN15 was reported by Farago et al.[13] Komura et al.[14] were the first to try the superconducting coils to provide precession field for the NSE in the late 1980s at the Kyoto research reactor in Japan.

The history

The proposal for an NSE instrument at the SNS at Oak Ridge National Lab began in the 2000s along with the construction of the SNS itself. It was driven by the Institute of the Solid State Physics (IFF now JCNS) of the Forschungszentrum Jülich, which was already involved for a long time in the manufacturing, operation, and scientific use of the NSE spectrometers at the Jülich research reactor DIDO, at the ILL, and in collaborations with other neutron sources, for example NIST.[15] The Memorandum of Understanding (MOU) for building the SNS-NSE was signed in February 2006 by the partners of ORNL and Forschungszentrum Jülich. The first echo at the new instrument was recorded in September 2009, followed by the start of the user operation in early 2010. For about a decade, the Forschungszentrum Jülich operated the instrument with its own staff as an "outpost" at the SNS, and by the end of 2020, the instrument and its operations had been transferred over to ORNL. Recently, some of the aging electronics and software components have been upgraded to

This is an open access article under the CC BY-NC license (http://creativecommons.org/licenses/by-nc/4.0/).

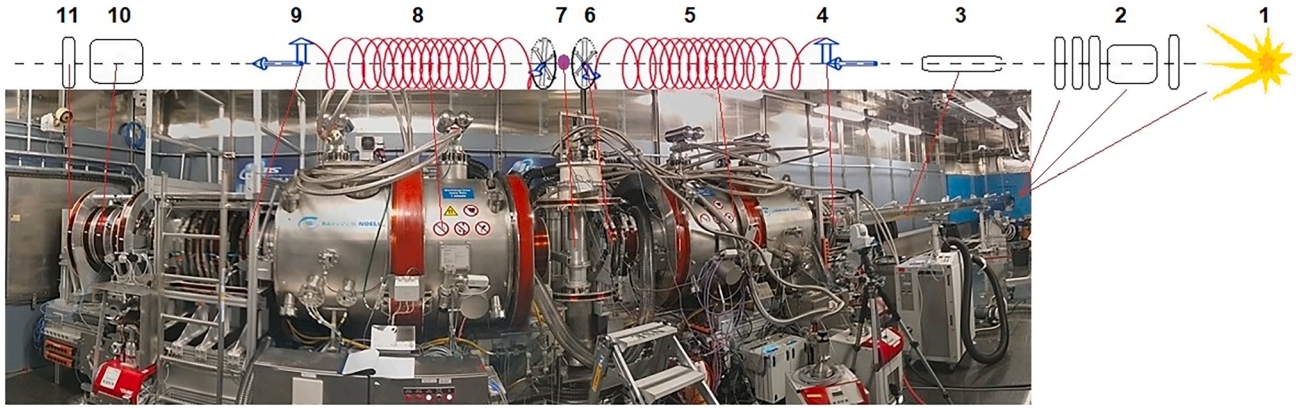

Figure 1. The SNS-NSE instrument at the Spallation Neutron Source and the neutron fly path schematic with the most important spectrometer components

From right to left: 1 = neutron source; 2 = choppers-bender-polarizer-shutter system; 3 = beam transport guides; 4 = pi/2 flipper for first 90° flip; 5 = first precession superconducting coil; 6 = pi flipper for 180° flip; 7 = sample area and sample environment (here the cryo-furnace is shown); 8 = second precession superconducting coil; 9 = pi/2 flipper for second 90° flip; 10 = analyzer; 11 = detector. (Note that portions of 3 as well as 2 and 1 are situated behind the blue shielding wall). Image: ORNL/Genevieve Martin.

maintain reliability and to address some of incompatibilities between Jülich and Oak Ridge data acquisitions and control systems. The SNS-NSE is now fully integrated into the ORNL SNS suite of instruments and is currently one of the two NSE instruments available in the Americas.

During the operation of the SNS-NSE since 2009, many experiments were carried out in the field of soft matter, biology, interface dynamics, and magnetic fluctuations, which came from international collaborations and from an increasingly growing community in the US. In this review, the development of the instrument from the first ideas to full user operation is traced. Scientific achievements, advancements, and highlights in various fields of science from the 1.5 decades of user operation are discussed and peculiarities and opportunities of NSE instrument operations at pulsed sources are presented, including advanced data acquisition and data reduction strategies.[16] The objective of this study is to provide a comprehensive overview of the scientific richness and diversity within the high-resolution neutron scattering community. In addition, the study will identify the future directions of research with the NSE and explore emerging trends and perspectives in this field.

HIGH RESOLUTION SPECTROSCOPY

Neutron spectroscopy can address a variety of scientific questions probing systems on very different time and length scales and employing an assortment of techniques. Small-angle neutron scattering (SANS) and neutron reflectometry (NR) are often used to provide structural insights into molecular samples, whereas the dynamics is then obtained by the NSE.

The domain of neutron spin echo spectroscopy covers a large area of length scales from atomic distances to length scales typical for membranes and macromolecules, and timescales spanning from picoseconds to 100's of nanoseconds, see Figure 2. This time window or, equivalently energy window of neV-μeV, is virtually impossible to reach by any other technique with comparable spatial resolution. The extremely sharp energy resolution of the NSE stems from the measurement principle of encoding and decoding of the neutron velocity before and after the scattering event. The velocity encoding/decoding process involves a very large number of precessions in a nearly perfectly symmetric magnetic field environment, which results in a polarization "echo".

The following is a brief overview of the working principle and the measuring principle of the neutron spin echo spectroscopy. The double differential cross section $\frac{d\sigma}{d\Omega dE_f}$ describes a scattering experiment. It is defined as the number of neutrons scattered (per unit of time) into a solid angle $d\Omega$ that have final energy between E_f and $E_f + dE_f$ and is typically given as[17]:

$$\frac{d\sigma}{d\Omega dE_f} = \mathcal{A}\frac{k_f}{k_i}\frac{1}{\hbar}S\left(\vec{Q},\omega\right) \qquad \text{(Equation 1)}$$

with the contrast factor $\mathcal{A}$, the incoming and outgoing scattering wave vectors k_i and k_f, respectively, and $S(\vec{Q},\omega)$ is the scattering function, which describes the spectral response of the sample to the neutron beam. The so-called scattering vector $\vec{Q} = \vec{k_i} - \vec{k_f}$ quantifies neutron momentum change and, $\hbar\omega = \Delta E$ ($\Delta E = E_i - E_f$) describes kinetic energy change between initial E_i and final state E_f of the neutron (Note that if the spin-echo approximation $\Delta E \ll E_i$ holds, k_f/k_i ratio is basically 1).

In NSE, a polarized neutron beam passes through a magnetic precession region before and after the scattering process at the sample. The velocity of each neutron is thereby encoded by a number of spin precessions, and decoded again after the scattering process. A change in neutron energy during the scattering (and hence in velocity) results in an additional phase angle of the corresponding individual neutron, or in a loss of polarization of the ensemble of neutrons of the beam. The degree of polarization measured at the detector then represents the intermediate scattering function $S(Q,t)$ of the sample at (Q,t) values given by the instrument settings of magnetic field and scattering angle.[2,12]

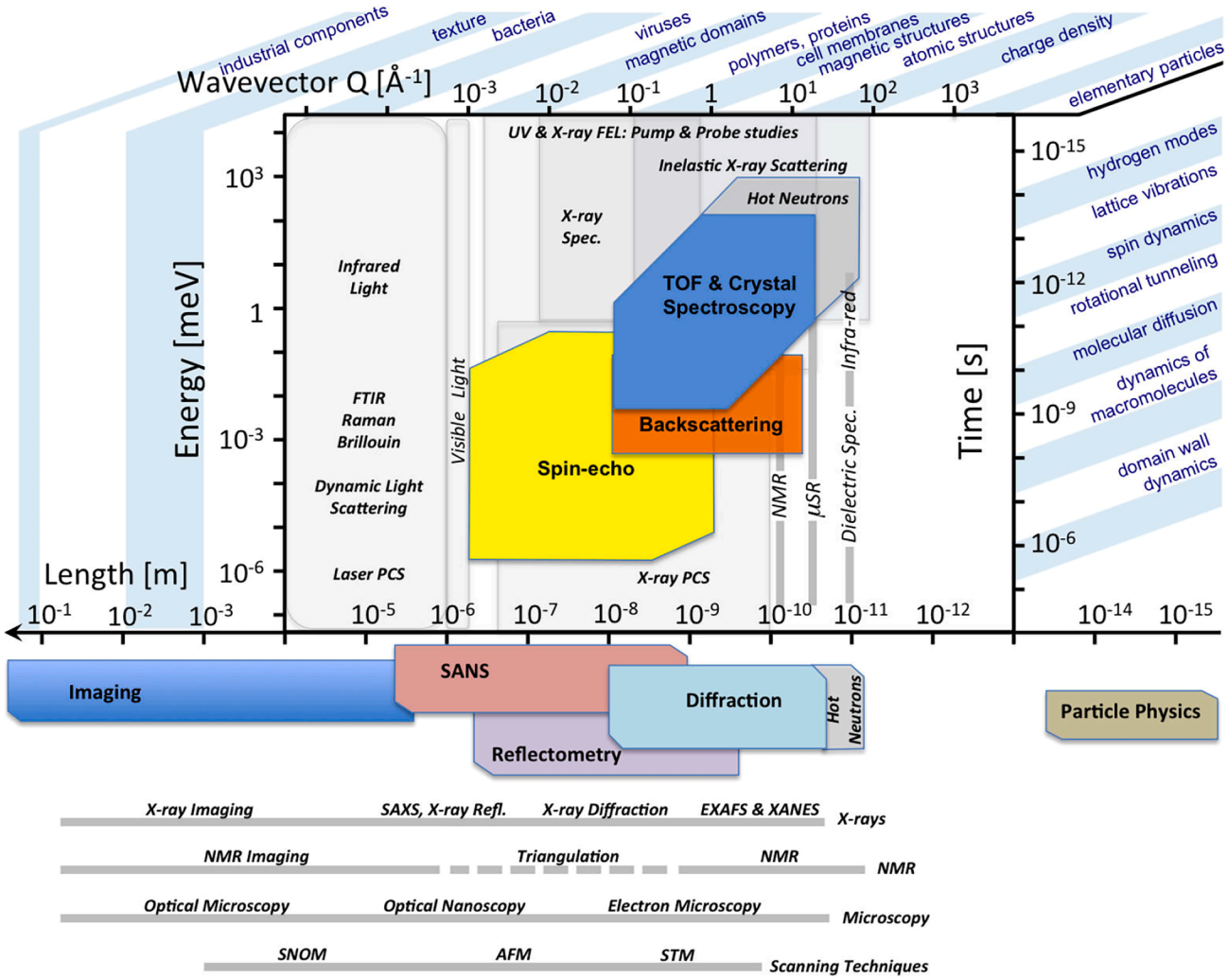

Figure 2. Length scales and timescales covered by different neutron scattering techniques and compared to complementary lab-based and X-ray scattering techniques

The yellow area NSE is covering in space and time is very important for large molecules and slow motions and provides together with the specific contrast conditions for neutron scattering a unique combination. Used by permission from ESS Technical Design Report 2013.

$$S(Q,t) = \int \cos(t\omega) S(Q,\omega) d\omega \qquad \text{(Equation 2)}$$

It is the cosine Fourier transform of the scattering function from the energy to the time domain, where the Fourier time is given by:

$$t = J\lambda^3 \frac{\gamma_n m_n^2}{2\pi h^2} \qquad \text{(Equation 3)}$$

and depends on instrumental parameters (through so-called field-integral J), the mass of the neutron, m_n, the gyromagnetic ratio γ_n, and the wavelength λ. The field integral is defined as $J = \int B d\ell$, where B is the magnetic field along the path ℓ of neutrons. Note the strong dependence of the Fourier time on the wavelength.

The sensitivity to minute velocity changes comes from the fact that even a small additional precession angle results in a loss of polarization of the final neutron echo with number of precessions reaching up to 10,000 to 100,000. This provides the sensitivity to velocity changes on the order of $\Delta v/v = 10^{-6}$ for neutron velocities in the range of $v = 250 - 1000$ m/s corresponding to wavelengths of $\lambda = 4 - 16$ Å.

The intermediate scattering function $S(Q,t)$ measured by NSE is described previously as the Fourier transform of the scattering function from energy into time domain. But it can be also regarded as the Fourier transform of the van Hove correlation function $G(r,t)$[18,19] from real space into the reciprocal space, which states how probable it is to find a particle at position r at time t provided another particle (atom) was initially at position 0 at time 0. This kind of correlations can be obtained from atomic trajectories from molecular dynamics (MD) simulations, where the

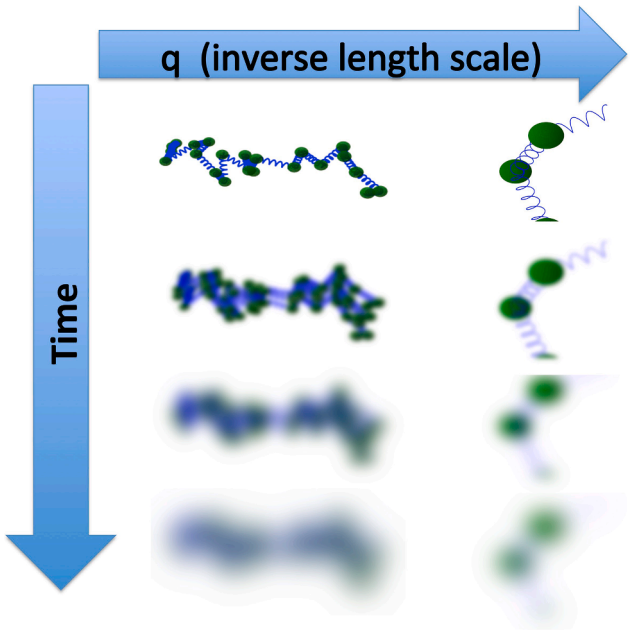

Figure 3. Illustration of the loss in knowledge with time on different length scales, which corresponds to the decaying intermediate scattering function $S(Q,t)$ measured with NSE
Adopted from Holderer et al.,[69] CC-BY 4.0.

position of each atom at each time step is known. This makes it possible to link MD to $S(Q,t)$ measured by NSE.

NSE provides information on the dynamics of molecules with a length-scale sensitivity provided by measuring $S(Q,t)$ at different scattering vectors Q corresponding to molecular length scales. This length-scale resolved dynamics in the domain shown in Figure 3 provides directly information on the molecular motion, which is complementary to other techniques such as X-ray photocorrelation spectroscopy (XPCS, similar length scales, larger timescales), dynamic light scattering (DLS, larger time and length scales), and pulse-field gradient NMR (also larger timescales) and additionally allows for contrast variation, i.e., labeling or hiding parts of a complex multi component system by isotope substitution (typically H-D).

The "art of NSE instrument development and construction" is now to provide precession regions for the full neutron beam in front of the sample and—symmetrically—for the scattered beam with a divergence as large as possible, here we achieved $\pm 2^{\circ}$; all neutrons need to experience the same magnetic field integral on their paths through the instrument with the relative precision of 10^{-6}. The innovative steps in the design and construction of the SNS-NSE in order to achieve this goal will be described in the following section.

THE INSTRUMENT

The NSE spectrometer at the SNS, shown in Figure 1, is principally of the classical IN11 type.[3] Three main innovations have been realized at the SNS-NSE, which contribute to its unique capabilities and which will be described in the following sections.

(1) Continuously changing wavelength (TOF)
(2) Superconducting solenoids
(3) Magnetic shielding

The superconducting coils and the magnetic shielding equips the SNS-NSE with an instrumental reliability and stability allowing to probe also smallest effects of changes in the relaxation rate (e.g., modified undulation spectra in microemulsions in the study by Lipfert et al.[20]).

Generally, the instrument is capable of serving the classical region of small scattering angles (extending small-angle neutron scattering into the time domain), and also going to scattering angles up to 79.5°, with a maximum scattering vector Q of 3.1 $Å^{-1}$, which makes atomic distances and dynamics in the area of glass physics accessible. For the complete list of instrument parameters please refer to the instrument website.[10]

Continuously changing wavelength (TOF)

The time-of-flight (TOF) NSE was already anticipated in 1979 by Ferenc Mezei,[12] and the first actual tests were done at ILL in early 2000's.[13] The addition of TOF allows for broader incoming wavelength band, larger ranges, and higher precision of measured wavevectors in a quasi-continuous way. It also comes with challenges, as all three flipper currents have to be ramped during each pulse to "keep up" with changing neutron wavelength. All other currents and magnets stay static, which implies that the Fourier time $\propto \lambda^3$ varies within each pulse. The longest wavelength together with the maximum useful field integral of 0.56 Tm (i.e., integrated magnetic field along the neutron path through one solenoid with acceptable inhomogeneity over the beam area) determines also the maximum achievable Fourier time (resolution) of the instrument, which is 130 ns for the wavelength band of 8–11 Å or 280 ns for the wavelength band from 11 to

14 Å (with decreasing intensity with increasing λ, hence the shortest wavelength band providing the needed resolution is normally chosen).

Full power of the TOF-NSE is displayed in combination with sophisticated evaluation software that can cope with this increased complexity of the data, see Zolnierczuk et al.[16] and "Data evaluation with TOF" section. As it is the case at the SNS-NSE, this new operation mode allows for a very efficient usage of the neutron pulse. Besides the accessible broad wavelength band in general, the TOF operation of NSE allows also for trading wavelength (and Q-) resolution versus counting statistics a posteriori by varying the time channel binning and hence deciding after the experiment for more steps in Q or smaller error bars, which on traditional instruments at continuous sources is fixed by the chosen wavelength band provided by the neutron velocity selector.

TOF operation in NSE spectroscopy means that for a typical setting of one wavelength band $\lambda = 5 - 8$ Å and a scattering angle of the second arm of the spectrometer of $2\Theta = 6.55^\circ$ the Q range varies almost linearly from 0.094 to 0.13 $Å^{-1}$ for this single setting throughout the pulse, while the maximum achievable Fourier time varies at the same time from $\sim$ 15 to 50 ns. With a single setting, one always covers simultaneously a range of Q and t, in contrast to an NSE based at a continuous (reactor) source, where at a single Q value a series of Fourier times has to be measured subsequently (one can expand the Q-coverage slightly by using a 2D detector, which is also the case of SNS-NSE). The technical price to pay is that instead of a static setting for a given Fourier time, as it is the case for a continuous source NSE, the flipper currents have to be ramped synchronously with each neutron pulse in order to assure the right flipper operation.

Superconducting main solenoids

NSE with superconducting coils was first attempted as a "proof of principle" at the Kyoto Reactor in late 1980's,[14] whereas the SNS-NSE is the first dedicated instrument employing main superconducting coils, see the study by Walter et al.[21] for the technical details. All prior NSE instruments (IN15 at ILL, NSE at Jülich DIDO Reactor, and NSE at NCNR - NIST Center for Neutron Research) had resistive main solenoids made of copper wires with water cooling to remove the heat. This required massive power supplies (up to 160 kW) and cooling water infrastructure. The advantage of superconducting coils is the geometric accuracy and the thermal stability (no expansion due to warming up during operation). The downside of using superconducting coils is a limited speed in ramping the currents, and the big mass required to keep at superconducting temperatures, which requires a continuous cooling. Two recently upgraded NSE instruments, the J-NSE "PHOENIX"[11] and its sister instrument at NCNR (CHRNS-NSE), followed the route of employing superconducting main solenoids. The SNS-NSE paved the way for further developments with optimized field shape by segmenting the main solenoid as for the J-NSE "PHOENIX" or the CHRNS-NSE. The SNS-NSE design with its rather compact main solenoids which are (as the successors as well) fully compensated for dipolar stray fields, a feature only possible with superconducting design due to geometrical constraints of the coils. This opens also the possibility to access large scattering angles without cross talk of the coils and therefore with minimal influences on the resolution of the instrument.

The extremely high-field homogeneity demanded by the NSE requires additional correction elements. The SNS-NSE instrument employs so-called "Pythagoras"-type correction coils[9] which were originally introduced at IN15 instrument at ILL (B. Farago, personal communication).

Magnetic shielding

Finally, the instrument cave serves primarily as a radiation protection barrier, but it also integrates a magnetic shield against fields from the surrounding environment. The magnetic shield[22] consists of a double layered wall made from μ-metal providing a shielding factor of 137 and makes the instrument immune to crane movements in the instrument hall or to the use of magnets at the neighboring instruments.

This unique and stable magnetic environment (see Figure 4), not realized at any other neutron scattering instrument so far, makes the instrument extremely stable and reliable as shown in Figure 5, and allows to measure very small changes in the intermediate scattering function. An example is the small but systematic variation of relaxation times of microemulsions due to the addition of tiny amounts of clay platelets.[20] The precision and high resolution of the NSE instrument lies in the sensitivity to phase angle variations before and after the scattering process at the sample. With some 10,000 precessions, a fraction of a single precession results then in a measurable loss in polarization. Variations on one solenoid in the range of some mG already can achieve such perturbances. Since this is much smaller than the earth magnetic field, this is already observed when large steel parts are moving, such as a crane, or if distant unshielded magnets are in operation. The magnetic shielding provides here a unique way of measurement stability. Additionally, also the radiation shielding of the room provides a very low neutron background. Especially for measurements with low scattering intensity, this aspect matters strongly and provides an advantage compared to instruments not enclosed into a protective hutch.

DATA EVALUATION WITH TOF

Neutron spin echo spectroscopy applies a spin flip sequence to the polarized neutron beam, which encodes the intermediate scattering function $S(Q,t)$ in the polarization at the last spin flipper. With a fixed wavelength and a rather broad wavelength spread $\Delta\lambda/\lambda = 0.1 - 0.2$, this allows to achieve high-energy resolution even with a moderately monochromatic neutron beam. The 10%–20% spread is typical for instruments operated at a reactor like, J-NSE "PHOENIX",[11] IN15,[23] or NIST-NSE[15] that use a mechanical velocity selector to filter the incoming wavelength. All magnetic fields in such a setup can be static and need to be varied only from one Fourier time setting to the next. The experimental sequence here comprises the choice of a scattering angle corresponding to a desired $\vec{Q}$-value and setting of currents such that the magnetic fields yield the aimed at Fourier time. The nominal scattering vector $\vec{Q}$ then is valid for the center of the detector. The only further $\vec{Q}$-variation stems

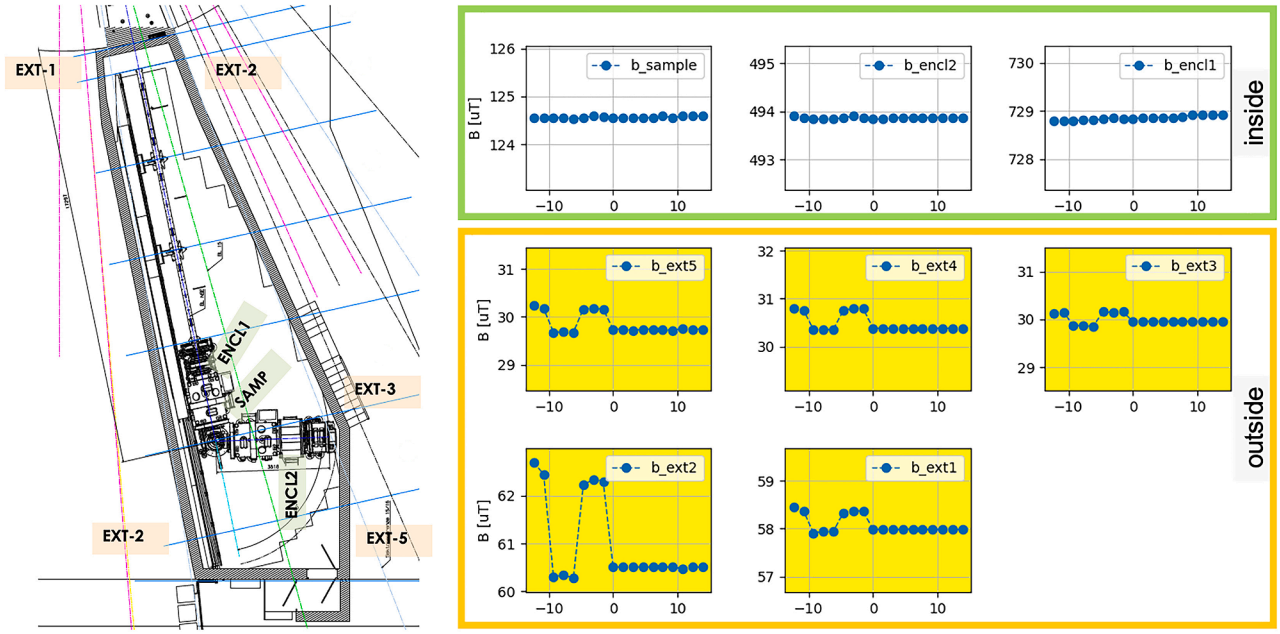

Figure 4. Field stability example

Left: magnetic field sensors locations inside (SAMP, ENCL1, and ENCL2) and outside (EXT1-EXT5) the experimental cave. Right: magnetic field as a function of phase point for the sensors outside and inside the cave. The magnetic field inside the cave remained stable despite the fact that the external sensors picked some field instability during the first few phase points.

from the 2D detector which covers some solid angle around the central spot.

TOF operation at an NSE spectrometer introduces more complexity in instrumentation as discussed in the "The instrument" section, but also in the data analysis and reduction. The wavelength spread during a pulse is typically much broader than for a continuous source experiment. In the case of the SNS-NSE, a wavelength band with a width of 3 Å is used (e.g., 5–8 Å or 8–11 Å to cover different Fourier time ranges). The width of the wavelength band is determined by the distance of the instrument from the source and the repetition rate of 60 Hz the source (the further away, the smaller the usable wavelength band in order to avoid overlap of the pulses). The broad wavelength band can be fully exploited with NSE since within each pulse the different wavelengths are well ordered, with the short wavelengths arriving first at the instrument, the longest wavelength last. This has two implications on the data evaluation. First, within each pulse the Fourier time t varies strongly from the beginning to the end of each pulse, since $t \propto \lambda^3$, secondly, according to Bragg's law, $Q = 4\pi/\lambda \sin(\Theta/2)$, also the momentum transfer Q varies within each pulse. This requires that each pulse is sliced into a number of frames (typically 42 in the case of SNS-NSE), and within each frame the intensity are histogrammed in corresponding (Q, t)-bins over many pulses. The broad wavelength band requires furthermore that the currents of the neutron spin flippers are adapted within each pulse with a saw tooth like current function. All other currents in the solenoids are kept constant because their large inductance forbids rapid variations. This implies the before mentioned variation of t within each pulse. A universal data evaluation procedure for classical NSE instruments at continuous and pulsed sources is described elsewhere.[16]

In summary, the operation of an NSE spectrometer at a pulsed source presents additional challenges to efficiently extract all information content on echo amplitudes from the neutron counts and opportunities to the data acquisition and reduction yielding an a posteriori to a (quasi) continuous (Q,t) access within the covered range. The flexibility available in data reduction is especially useful if the samples are structured with structure factor peaks within the Q range under investigation. Varying the Q-resolution by varying the binning allows to check influences of Bragg peaks or "de Gennes narrowing" close to maxima in the structure factor, relevant e.g., in lamellar phases as described in "Polymers" section with nanoconfinement, or in "Interface dynamics" section under grazing incidence conditions, where Q-resolution matters as much as statistics and where it is difficult to assess beforehand the exact requirements of each side. Depending on wavelength, time channel binning, pixel binning, and counting statistics, the TOF structure allows to achieve a Q resolution of better than $\Delta Q = 0.003$ Å^{-1}.

SCIENTIFIC ACHIEVEMENTS

The following section presents a selection of illustrative experiments conducted at the SNS-NSE, spanning various scientific disciplines. The primary focus research conducted at the SNS-NSE is soft matter science, as the time and length scales of the technique align perfectly with those of thermally driven fluctuations in macromolecules, including polymers, proteins, and

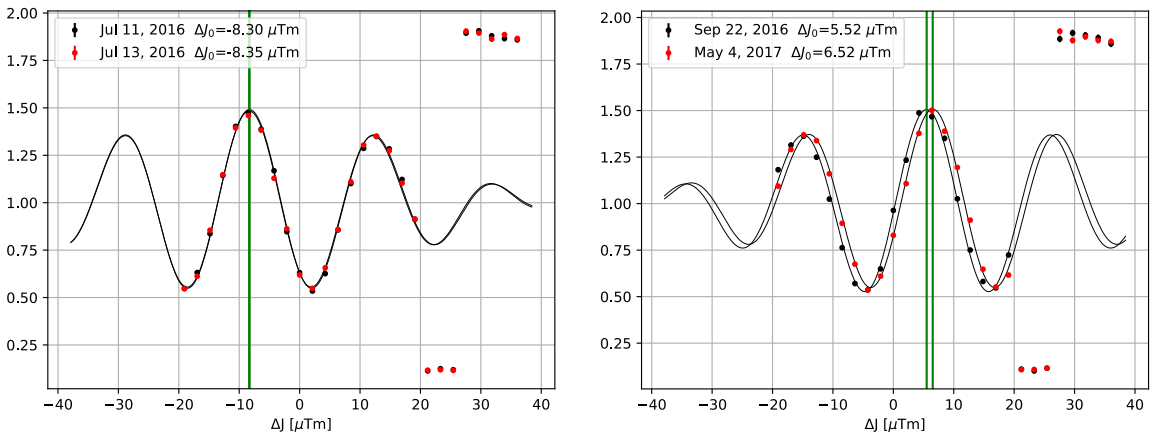

Figure 5. Phase stability examples at field integral = 0.53 Tm (τ_{max} = 50 ns)

Phase shift $\Delta J_0 = 0.05\ \mu$Tm corresponding to neutron precession angle of about 3°, as observed in 2 days (left figure), and $\Delta J_0 = 1\ \mu$Tm corresponding to neutron precession angle of about 22°, as observed in the span of about 7 months (right figure). Instrument settings: wavelength band $\lambda = 5 - 8$Å, scattering angle $2\theta =$ 10.2 deg (left figure) and $2\theta = 5.8$ deg (right figure). The echos show an integral over the complete wavelength band, which causes the decaying envelope of the echo curves.

biological membranes. Paramagnetic scattering represents another scientific domain of NSE, encompassing fluctuations in spin glasses and spin ice.

The unique instrumental aspects, such as the magnetic shielding, the pulsed beam, and the superconducting coils allowed to establish new trends and were driver for new developments, for example concerning advanced optical components for grazing interface measurements ("Interface dynamics" section and led to the nucleus of the formation of new scientific collaborations and communities interested in high resolution dynamics ("Paramagnetic" section).

The dynamics of polymers, proteins, and membranes can be described in terms of a Langevin equation of motion. For a single spherical particle, this would result in Brownian motion with a diffusive like behavior for the intermediate scattering function of the form $S(Q,t) \propto \exp(-DQ^2t)$ with the Stokes-Einstein diffusion constant D. The Q^2-dependence is characteristic for diffusive processes and can be studied with the NSE capabilities of selecting different Q-values.

For more complex structures, the Langevin equation can be solved and the intermediate scattering function can be calculated using coarse grained polymer models, such as the bead-spring model depicted in Figure 6A. Typical examples are the Rouse model for polymer melts or the Zimm model for polymers in a viscous medium (for more details we refer to the literature[24,25]). Normal mode analysis[26] is applied to study the dynamics of large proteins with subdomains, which may fluctuate with respect to each other (see Figure 6B). There is a transition between rigid subdomain motion of proteins and segmental motion of flexible polymer chains, where both coarse grained and normal mode approaches can be tested. In some cases modifications to the Zimm model can describe the internal dynamics. This is especially true for intrinsically disordered proteins, where the Zimm model is modified to contain not only the friction of the surrounding medium (via the viscosity) but also chain-internal friction with a second relaxation time. By analyzing the Q-dependence and the curve shape of the intermediate scattering function, these differences and relaxation times can be extracted.

Finally, for membrane sheets fluctuating in a viscous environment (Figure 6C), the Zilman-Granek model is often applied. It is most commonly used to study biological membranes.[27]

Polymers

Since the inception of NSE, the study of dynamics in soft matter systems has been one of the strongest scientific areas. For all samples where the molecular scale structure can be analyzed with SANS, the motion within such samples (if existent) can be studied on the same length scales using NSE. There are two main modi operandi: one is to measure the coherent intermediate structure factor $S(Q,t)_c$ in samples containing a few protonated molecules (polymers, proteins …) dispersed in a predominantly deuterated matrix (D_2 O, deuterated polymer matrix). The other is to target the incoherent structure factor $S(Q,t)_i$ where the proton scattering dominates (and cause a spin flip of the polarization). In reality, both contributions are present, with one usually prevailing. The two structure factors, $S(Q,t)_c$ and $S(Q,t)_i$, correspond to the distinct and self parts of the van Hove correlation function. Modeling has to take these components into account accordingly.

Some prominent examples from the SNS-NSE are highlighted in the following. Looking ahead, the trend seems to point toward increasing complexity in molecular architecture, e.g., polymers with topological peculiarities, such as ring polymers, stars etc., or microgels with specific cross-link properties, such as homogeneous, heterogeneous, physical or chemical cross-links, or regular meshes. More complex environments with constraints due to interfaces, pores, or other components represent an area where more industrially relevant questions may arise. From the technical standpoint, the data analysis remains a bottleneck due to the complexity of the obtained correlation

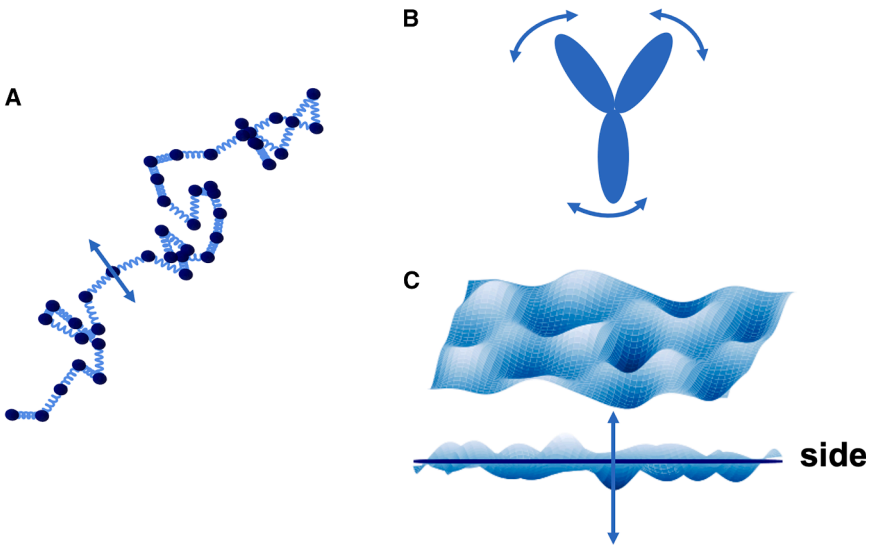

Figure 6. Examples of motion which can be studied with NSE

(A) polymer segmental dynamics, here with a polymer chain represented in the bead-spring-model, which also is applicable to the dynamics of intrinsically disordered proteins as natural polymers.

(B) Sub-domain motion of proteins, as e.g., the hinge-motion in Y-shaped immunoglobulins.

(C) Membrane height fluctuations, as e.g., in microemulsions or biologically relevant phospholipid membranes.

functions. This challenge may be tackled through new modeling or simulation capabilities.

Polymer dynamics in the melt and in solution

The classical NSE topic of polymer dynamics in the melt and in solution has been extensively described by Richter et al.[25] More recent examples from the SNS-NSE comprise the dynamics of polymers in solution with more complex architecture, such as gels, microgels, and the very recent single-chain nanoparticles (scNPs). The latter are regarded as an interesting synthetic model for biomacromolecules allowing to study specific details in interaction and functionality. The dynamics of such particles is more complex than that of a single linear polymer chain in solution. E.g., internal interactions to be ascribed to, internal friction due to interactions within the particle may become important. An example of scNPs studied at the SNS-NSE is amphiphilic scNPs with non-covalent interactions.[28] Microgels, as another class of more complex polymers in solution, are cross-linked polymer chains, which form a network with constant or variable crosslink density, which is structurally hardly discernible, but has an influence on the segmental dynamics of the polymer chains. Homogeneously and heterogeneously crosslinked PNIPAM microgels have been studied by Witte et al.[29] Adding electrolytes to microgels can lead to a suppression of segmental fluctuations, as has been observed in the study by Pasini et al.[30] Concentrated solutions of PNIPAM show interesting behavior of volume phase transitions due to temperature changes and a similar behavior due to changes in solvent quality, the so called co-nonsolvency effect, when certain concentrations of alcohol and water lead to a polymer collapse, while alcohol and water are both good solvents for the polymer. The behavior and collapse also implies changes in the polymer chain dynamics, analyzed by Raftopoulos et al.[31] The dynamics of very well defined gels in terms of cross-link architecture are studied by Hiroi et al.,[32,33] which is illustratively depicted in Figure 7. It turned out in these investigations, that the diffusive like density fluctuations with a characteristic Q^2-dependence of the relaxation rate dominate more in disordered gels, while ordered tetra-PEG gels show Zimm dynamics of ideal polymer chains already at larger length scales.

Besides chemical cross-links with chemical bonds at the connecting points, also weaker physical crosslinks can form gels, for example by ionizable groups, with a dynamic connection within the network, which might easier break and re-connect. Such heterogeneous networks with ionizable groups have different intra-cluster and network dynamics, which has been observed with NSE and correlated to molecular dynamics simulations.[34,35]

Nanoconfinement in polymer dynamics

The subject of dynamic phenomena in polymer melts induced by interactions with a confining surface is a topic of considerable discussion in the literature. Krutyeva et al.[36] this topic is addressed through neutron spin echo experiments. The NSE analysis revealed the presence of an anchored surface layer, wherein the polymer chains exhibit mobilities that differ from the observations made in previous literature,[37] which had described these chains as being in a glassy state. The polymer dynamics in confinement can be described as consisting of two phases. The first of these is identical to the bulk polymer, while the second is partly anchored at the surface. The latter phase exerts a strong topological interaction, confining further chains that are not in direct contact with the surface. These form the interphase, which has been the subject of much discussion in the literature. It is characterized by the impediment of full chain relaxation through the interaction with the anchored chains.

NSE combined with MD simulations

Length scale dependence of block copolymer dynamics. Polymer dynamics has consistently served as a pivotal scientific domain for NSE. The most recent experiments comprise studies of block copolymers (BCPs) with NSE, SANS, and combined molecular dynamics (MD) simulations. The objective is to gain a deeper comprehension of the influence exerted by the chain dynamics of the interfacial block. The block copolymers formed a glassy block and a rubbery block. The latter was protonated in part to highlight the region in proximity to the glassy block interface or at a greater distance. The contrast variation study revealed that the interfacial rubbery block was confined to layered morphologies and exhibited markedly slower dynamics than the chain-end rubbery block, which was dispersed in the rubbery

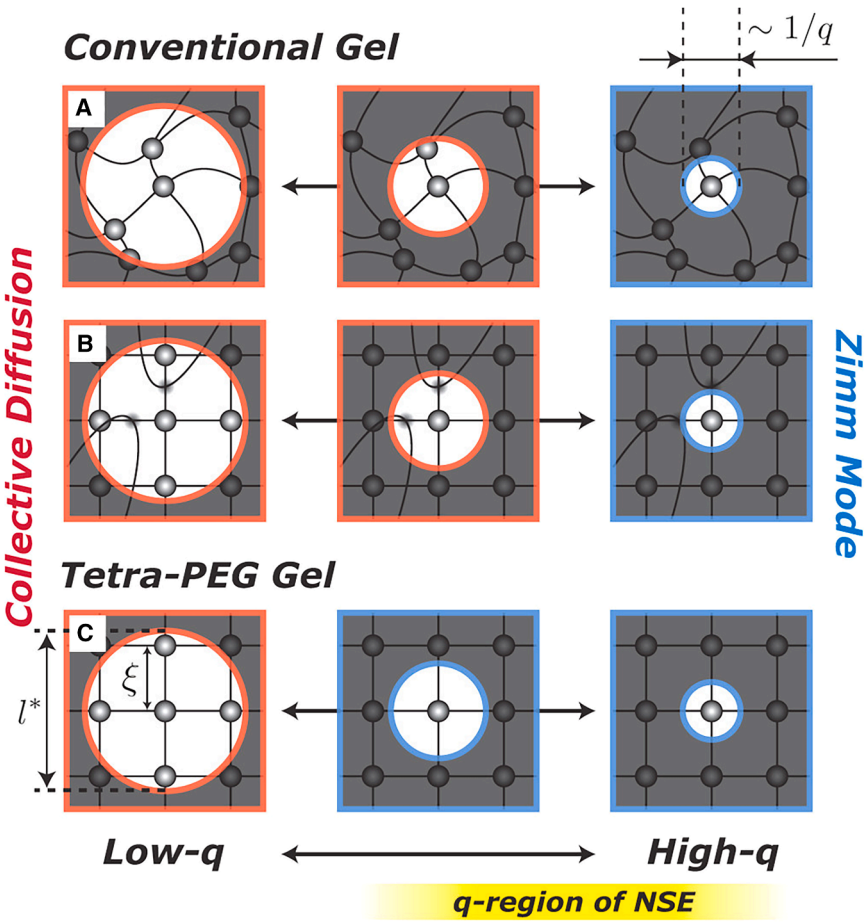

Figure 7. Dynamics probed in gels of different architecture can be probed in detail on length scales of single segments to larger gel regions

Dynamics measured by NSE shows the transition from collective diffusion stemming from density fluctuations at length scales above the mesh size, to Zimm-like single chain dynamics if zoomed inside the gel, when only single segments are observed, with the transition depending on the degree of order of the crosslinks. Lower order (A) determined by cross links and (B) additionally by entanglements results in stronger density fluctuations compared to the well defined cross-link distances in (C). Reprinted with permission from.[32] Copyright 2014 American Chemical Society.

matrix. NSE as well as MD allowed to obtain segmental relaxation rates, for NSE it is determined by the labeling scheme with partly deuterating different sections of the BCP, MD allows to select the corresponding parts in the simulation box. MD allows in this respect an experimentally verified molecular or atomistic view into the sample. Obtaining segmental relaxation times from different parts of the BCP is a strength of NSE experiments. The interfacial rubbery block exhibited reduced dynamical relaxation in comparison to that observed at the chain end. Additionally, it demonstrated a critical length scale dependence. Dynamical slowing was only evident at length scales that were considerably larger than the characteristic segmental length. Furthermore, the discrepancy between interfacial and chain-end dynamics increased with increasing length.[38]

Network formation by ionic clusters. The insights about polymer systems obtained from NSE can be significantly enhanced when coupled with MD simulations. An example is a recent paper[34] on the polymer networks formed by crosslinking polymers via ionic clusters. The MD simulations when coupled with NSE measurements allow first to validate the simulations as the agreement between the NSE and MD has been shown to be remarkable and then the simulations can be carried beyond the scales that are attainable by the NSE. This allowed to identify the dynamics within ionic clusters of a model, highly swollen ionic polymer network and provide a direct correlation between intrinsic dynamics of the ionic assemblies. It also demonstrates how the MD simulations and NSE experiments can work in tandem to provide new information not otherwise attainable by experimental efforts.

In Figure 8 the comparison between S (Q,t) from NSE experiments with that from MD simulations for different solvent conditions and hence different ionic clustering of the gel is shown, with an excellent agreement between simulation and experimental relaxation times.

Interface dynamics

Interfaces are ubiquitous in biological and soft matter materials, and also the motion and thermal fluctuations in the vicinity of interfaces play an important role. Besides interfaces in bulk samples, such as polymer melts in oriented cylinders in an alumina matrix,[36,39] also flat interfaces in a geometry similar to grazing incidence small-angle neutron scattering (GISANS) can be explored, named grazing incidence NSE spectroscopy (GINSES).[40,41] The advantage of such experiments at the SNS-NSE is 2-fold. First, the magnetically shielded room provides a very stable environment in terms of slow magnetic field variation (typically less than 1 mG even when strong magnets are used nearby), as well as radiation from other instruments. Secondly, the superconducting main coils provide also internally a stable geometry which does not depend on operation status, i.e., no thermal expansion due to heating of coils is present, which would otherwise result in possible phase shifts. The intensity in this operation mode is very low, typically some counts per second on the detector, which requires long acquisition times of several 100s of seconds per detector image.

Critical dynamics of 3-methyl pyridine/D2O mixtures without and with antagonistic salt

Confinement in fluids may be obtained in multicomponent systems. For example, binary Ising fluids show interfaces between the two components due to critical composition fluctuations near the phase boundary. Such an Ising system is 3-methyl

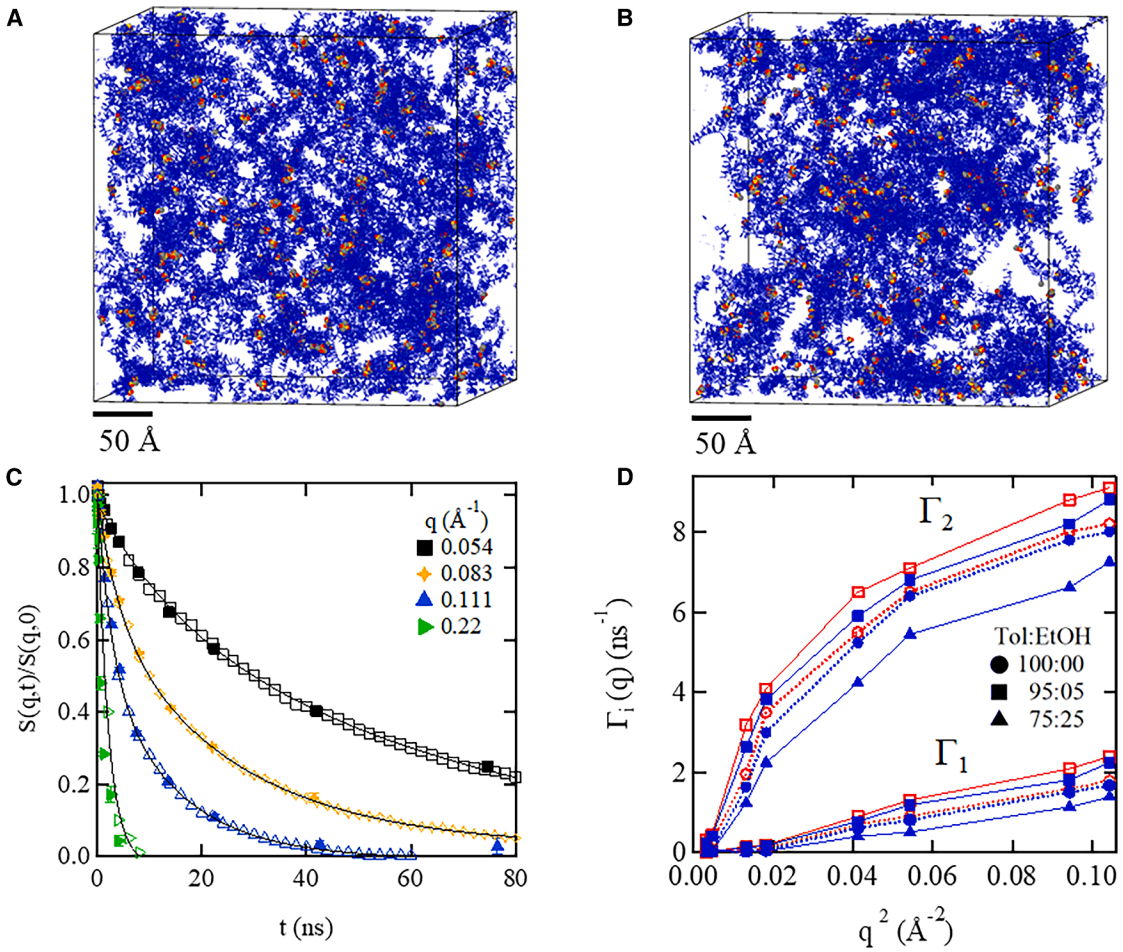

Figure 8. An example of NSE inspired MD simulations

The formation of stable ionic clusters linking the polymer network could be visualized and separated into the different components by MD simulations, while the mobile network dynamics measured with NSE and simulated with MD match perfectly and allow to validate the MD simulation.

(A and B) The molecular configuration after a long MD run for two different solvents.

(C) Comparison of the experimental S(Q,t) from NSE with that calculated from MD simulations and shows the excellent agreement between the two.

(D) The corresponding relaxation rates for different solvent conditions are presented with simulations in blue and NSE experiments in red. Reprinted with permission from Wijesinghe et al.[34] Copyright 2024 American Physical Society.

pyridine (3MP or 3-picolin) and D_2O with a three-dimensional (3D) ising criticality. Adding antagonistic salt additional charge fluctuations reduce the dimensionality to a 2D ising criticality.[42] NSE experiments together with SANS and dynamic light scattering allowed to observe the critical dynamics of these systems. The 2D case with the antagonistic salt showed a higher mobility, which might be relevant for applications where ionic transport is important.

Grazing Incidence NSE Spectroscopy

The geometry in GINSES (as in GISANS) requires a slit collimation (in GINSES in y-direction perpendicular to the flight path); the sample cell is typically a flat silicon block where the sample is in a bath behind (see Figure 9). The beam hits the silicon-sample interface under a shallow angle below the critical angle, resulting in an evanescent neutron wave reaching into the sample. The scattering of this evanescent wave is recorded when moving the detector to a Q-position which is off-specular in Q_z direction. The penetration of the evanescent wave depends on the scattering length density (SLD) difference between silicon substrate and sample, the neutron wavelength and the angle of incidence. The broad wavelength spectrum with $\Delta\lambda = 0.3$ nm requires some attention. Within one pulse, the penetration depth varies, which would result in a smearing of the distance to the interface where the dynamics is probed. To probe a single penetration depth for all wavelengths of a neutron pulse, a neutron prism has been used in the case of the SNS-NSE.[43] This allows significantly to simplify the data interpretation. A second neutron optical improvement of the GINSES technique also applied at the most recent experiments at the SNS-NSE is the use of neutron resonator structures at the Si-sample interface, which sharpen the evanescent wave and increase the intensity in the vicinity of the interface.

Scientific examples probed at the interface are surfactant membranes in microemulsions which orient at the interface

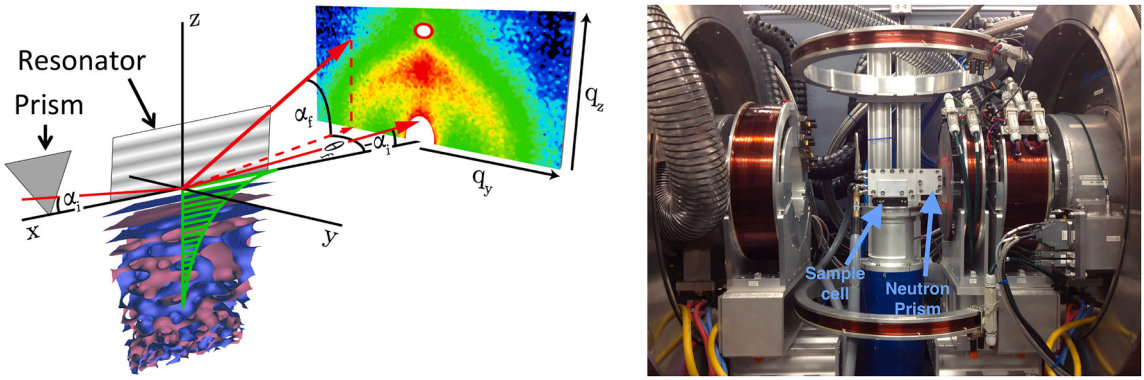

Figure 9. Grazing Incidence NSE Spectroscopy example

Left: neutron optical components used with the GINSES setup comprise neutron prisms made from MgF_2 and resonator structures at the interface made from several Pt/Ti layers

The sample shown here is a bicontinuous microemulsion forming lamellar structures in the vicinity of the interface, and the GISANS detector image. GINSES experiments are usually performed off-specular in the q_z direction. From Frielinghaus et al.,[44] CC-BY 4.0. Right: photo of the sample stage with the reflectometry type sample cell and the holder for the neutron prism.

and show a modified undulation mode spectrum,[45,46] and lipid bilayer stacks, which, due to their mechanical properties, even can show oscillating signals of elastic modes,[40,41] which can be rationalized in terms of a dynamic extension[47] of the calculation of the structure factor of a membrane stack.[48] Figure 10 shows the intermediate scattering function in such a case measured at the SNS-NSE.

Especially the GINSES experiments profit from the magnetic shielding and the low neutron background in the instrument hutch. Due to the restricted beam width and the scattering only from an interface layer, the count rate is very low, of the order of some 10 counts per second. With the low neutron background and magnetically stable environment such experiments become feasible. It also is an example where science driven

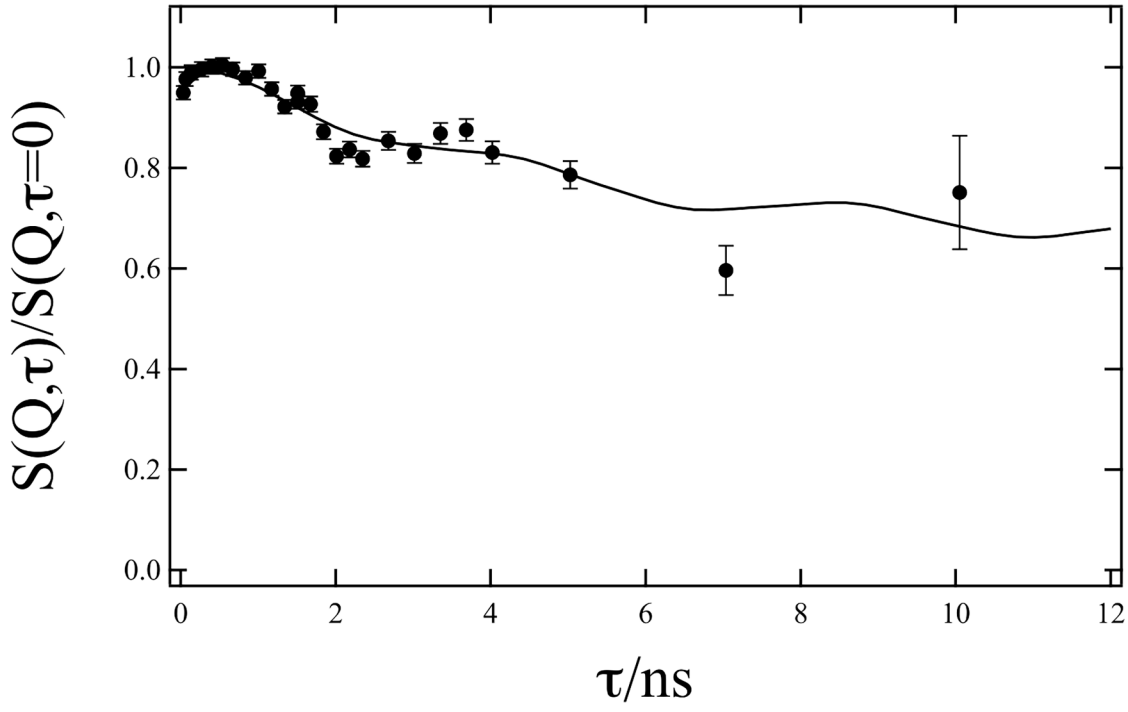

Figure 10. Intermediate scattering function from a stack of SoyPC double layers, showing an oscillatory decay well explained by theory.[47]

The very low count rate in this geometry require also a very low neutron background and magnetically stable environment, both present at the SNS-NSE. Figure from Jaksch et al.,[40] CC-BY 4.0.

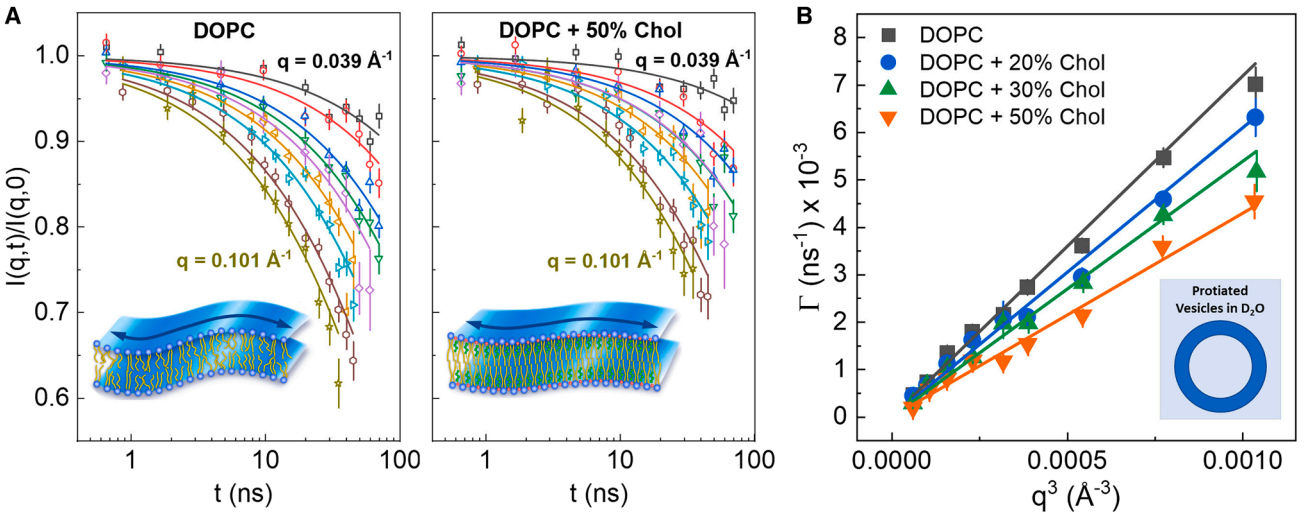

Figure 11. Change in membrane relaxation by the addition of cholesterol has been analyzed with the SNS-NSE

(A) S(Q,t) of DOPC phospholipid vesicles measured with the SNS-NSE.

(B) The relaxation rate, plotted in (B) decreases with increasing cholesterol contents, which is interpreted as a stiffening of the DOPC membrane. Reprinted by permission from Chakraborty et al.[52]

instrumentation with the new optical components lead to advancements from which the high-resolution community can profit in the future.

Biology

From complex architectures in polymeric systems, it is a small step to dynamics in biological systems; here, NSE plays an important role especially concerning the dynamics of proteins and of biological membranes. Intrinsically disordered proteins, for example, behave similar to polymers in solution and may be treated with similar models known from the polymer physics field or modified versions, such as the Zimm model or the Zimm model including internal friction (ZIF-model),[24,49,50] which described the dynamics of denatured apomyoglobin.[51] On the side of membrane dynamics, the strength of NSE is to measure the bending elasticity of membranes which are thermally fluctuating, such as phospholipid membranes. This allows to analyze changes of the elasticity due to the insertion of additives such as membrane proteins, drugs etc.

Similar to the technical statement in "Polymers" section, also in the case of biological systems the bottleneck is the demanding data analysis, be it in the case of large scale domain motion, which requires usually extensive modeling for example with normal mode analysis, or in the case of membrane dynamics. If it comes to even more complex systems like protein-membrane interactions, the future certainly will bring MD simulations and experiments closer together, as we can already see in first applications. Some prominent examples from the area of biology are presented in the following.

Membrane dynamics

One prominent example from the SNS-NSE is the observation of a stiffening effect of cholesterol.[52] Figure 11 depicts of how a change in cholesterol contents influences the membrane relaxation and allows to discuss effects on the membrane elasticity or fluidity. The change in membrane elasticity may also play a role in the interaction of myelin basic protein with the myelin sheath.[53] The elasticity of pulmonary surfactant may be altered by medium chain triglycerides from e-cigarettes, the effect could be analyzed with the SNS-NSE.[54] Peptide membrane interactions have been studied with different peptides, which are capable to modify the membrane fluctuations and elasticity, e.g., making the membrane more rigid when the peptide is in certain conformations.[55] Transmembrane insertion of peptides in a model membrane reduced the rate of thickness fluctuations and increased the membrane viscosity.[56] Lipid vesicles may also be controlled and modified by salt addition[57] which changes the elasticity, or by adding polymers, introducing morphology changes from unilamellar to multilamellar vesicles.[58]

Mechanical properties of nanoscopic lipid domains

The lipid raft hypothesis offers insights into the organization of proteins and lipids within cell membranes, elucidating the mechanisms through which these structures facilitate vital cellular processes. By integrating contrast matching techniques with inelastic neutron scattering, the bending moduli of lipid domains can be calculated, see Figure 12. In-register lipid domains within ULVs exhibit a distinctly different bending modulus compared to the surrounding continuous bilayer.[59]

Influence of a short antimicrobial peptide on charged lipid bilayer: A case study on aurein 1.2 peptide

The interaction of a short antimicrobial peptide, aurein, with a charged lipid bilayer is the subject of this study. Neutron membrane diffraction demonstrates that the peptide is situated at the surface of the bilayer. NSE spectrometry illustrates how aurein alters the moduli. The findings indicate that aurein does not induce membrane disintegration at low concentrations. The peptide modifies membranes through a mechanism of domain formation.[60]

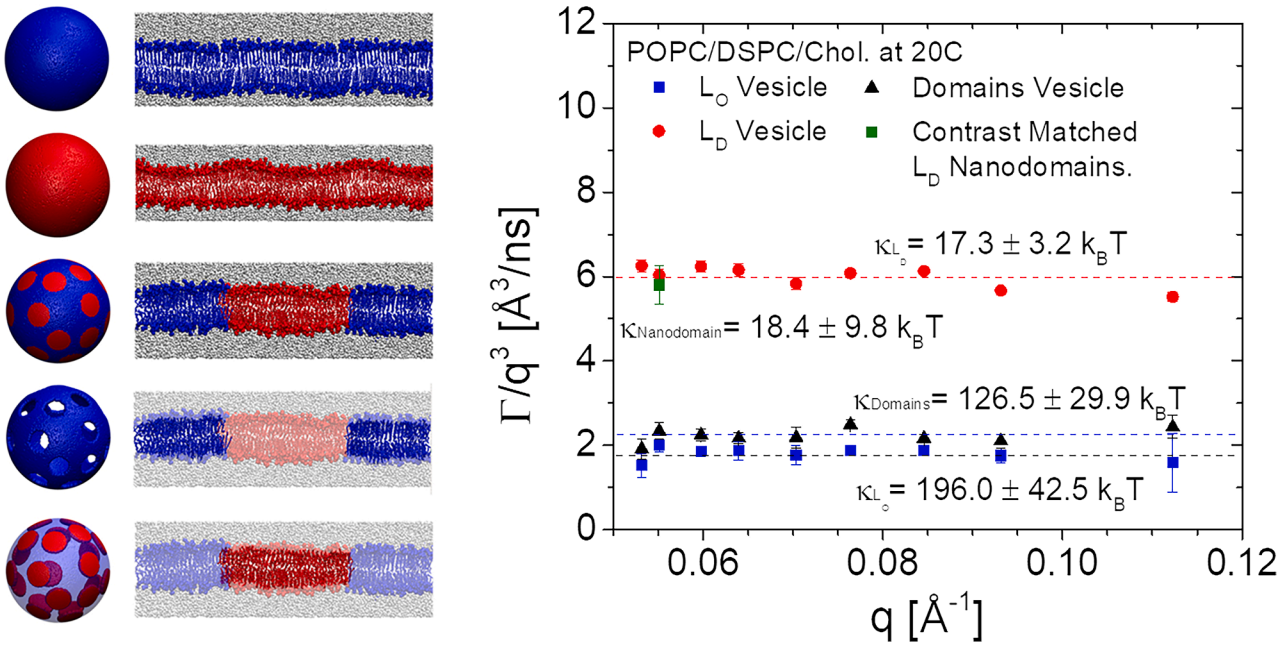

Figure 12. Lipid rafts studied with neutron scattering showcasing the power of contrast matching

The transparent colors on the left indicate the regions that were contrast matched, making them "invisible" to neutrons. The bending moduli for different regions are shown on the right. Adopted by permission from Nickels et al.[59] Copyright 2015 American Chemical Society.

Dynamics of thylakoid membranes

Thylakoid membranes (Figure 13) are the backbone of photosynthetic machinery in both algae and higher plants. These are flattened lipid membranes containing large proteins, enclosed in chloroplasts structures in plants and eukaryotic algae or floating freely within the peripheral region of the cell cytoplasm in prokaryotes. In these two studies, NSE spectroscopy was used to characterize for the first time the flexibility and dynamics of cyanobacterial thylakoid membranes and the dependence of these membranes dynamics on illumination conditions and chemical stress in living blue-green algae.[61,62] A direct relation between the thylakoid membrane motion *in vivo* and the photosynthetic activity was observed and described as basic undulatory membrane motion plus excess dynamics arising from correlations between very closely appressed thylakoids. The electron transfer chain between photosynthetic centers, the alleviation of electrochemical gradient (H+) and the modulation of proteins diffusion within the restricted space of the lumenal compartment explain the significant membrane dynamics difference between light and dark condition (approximately 4x faster in the dark than in light).

The same system was later submitted to chemical treatment by a well-known herbicide, DCMU (3-(3,4-dichlorophenyl)-1,1-dimethylurea),[62] an herbicide that suppresses the photosynthetic electron transfer. It was found that the disrupted thylakoids are 1.5x more rigid than the native membranes during dark, while in light they are 1.87x more flexible. The disrupted electron transfer chain and the decreased proton motive force within the lumenal space explain once more the variations observed in the mechanical properties of the membranes. This supports the hypothesis that photosynthesis plays a role in the mechanical dynamics of thylakoids and is quantitatively affected by the presence of herbicide. Both these studies performed at SNS-NSE, Stingaciu et al.[61] and Stingaciu et al.,[62] shed new light onto the potential role of lipid bilayer membrane dynamics in life-sustaining processes such as photosynthesis and open a new field of research for unique applications of the NSE spectroscopy technique.

Paramagnetic

Since neutrons have a magnetic moment, NSE can also be used to investigate paramagnetic scattering dynamics. Examples include spin glasses and more complex topological spin structures. Because magnetic scattering involves a π-flip, the main experimental change is to switch off the instrument π-flipper and let the sample do this part of the experiment. What starts as a relatively simple experiment can, in practice, become rather time consuming, as magnetic scattering is typically weak and often requires specialized sample environment, such as cryostats (sometimes operating down to 1 K). It is therefore a probably an area of NSE where new samples (with topological spin states or magnetic memory applications) might provide new possibilities, where the dynamics of > 1 ns is primarily accessed via NSE. Two examples from the previous studies are presented in the following text.

Magnetic charge defects mediated conductivity in artificial honeycomb spin ice

Controlling the electrical conductivity by magnetic charge-mediated conduction is a major development for spintronics

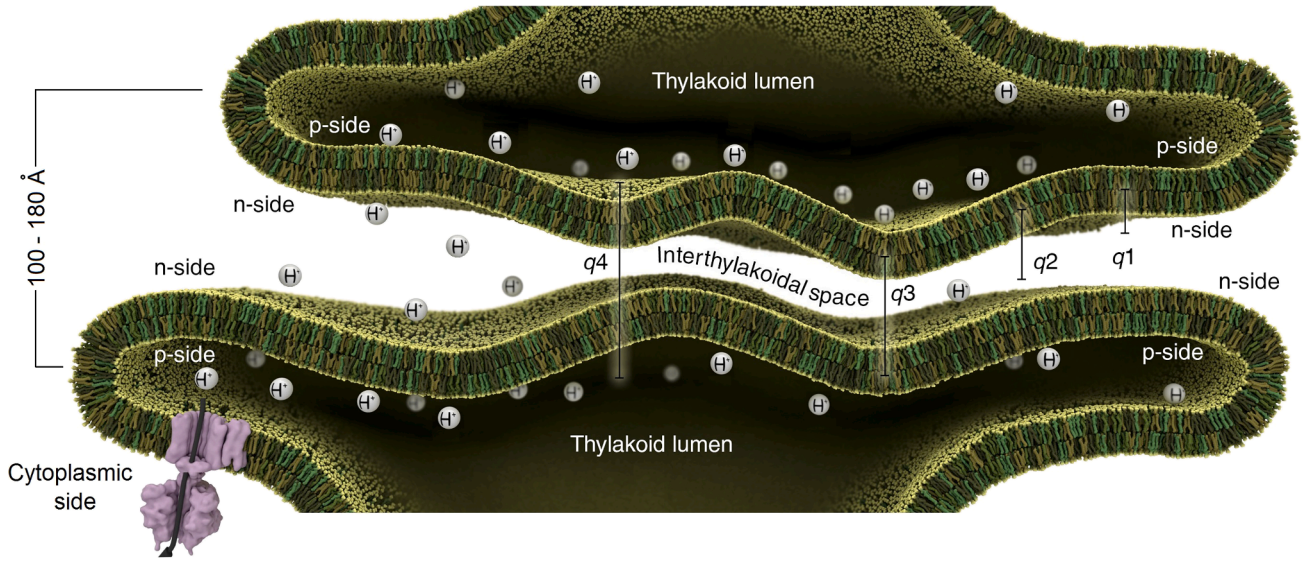

Figure 13. Schematic of thylakoid membrane morphology

From q1 to q4 a larger distance within the interthylakoidal space is sampled and different relaxation behavior is observed. The excess of protons H^+ in the lumen results in restricted membrane mobility during light. At dark, H^+ pressure is alleviated by chemiosmosis and the membranes undulate freely resulting in higher relaxation rates and excess dynamics. The purple feature is the ATP-Synthase responsible for moving the electrochemical gradient. Figure from Stingaciu et al.,[61] CC-BY 4.0.

applications. This has been demonstrated at low temperatures $\leq$ 15*K* in bulk spin-ice compounds in the early 2000, and further developed at SNS-NSE for 2D-systems and confined geometries. Nanoengineered honeycombs (Figure 14) made of single-domain magnetic elements (permalloy, Ni0.81Fe0.19) offer flexibility in tuning the element size, which insures flexibility in tuning the inter-elemental dipolar interaction energy, and were exploited to generate magnetic charge defects at the room temperature. Topological magnetic charges served as the origin of magnetic monopoles that traverse the underlying lattice flowing between nearest-neighbor or next-nearest-neighbor with high integer charge. Quantitative investigation of magnetic charge defects dynamics using NSE revealed sub-ns relaxation times comparable to the relaxation of monopoles in bulk spin ices, showing how the electrical conductivity is propelled by more than an order of magnitude as the temperature increases.[63]

Persistent dynamic magnetic state in artificial honeycomb spin ice

The magnetic flux on the honeycomb vertices was observed to be non-vanishing. The thermally tunable permalloy 2D-lattices exhibit a perpetual dynamic state in the absence of any external magnetic field or electric current. The kinetic process remained unchanged at low temperature (in negligible thermal fluctuation) due to self-propelled magnetic charge defects relaxation. Dynamic Monte-Carlo and classical micromagnetic simulations revealed the existence of perpetually active particles, quantum-type entities in their nature that share many traits with magnetic monopoles and magnons.[64] Moreover, synergistic studies of constricted nanomagnets with no net magnetization, made of antiferromagnetic neodymium thin films in the same honeycomb motif, point toward a persistent relaxation phenomena of chiral vortex loop-shaped topological quasiparticles that infers the same dynamical properties in neodymium nanostructure as in its ferromagnetic counterparts (permalloys).[65]

PERSPECTIVES

NSE spectroscopy covers the range of thermally driven motion, which is difficult to reach with any other method, but which is relevant in the domain of biology and soft matter, since large domain motions of proteins, membranes, and macromolecules lie exactly within this region of time and length scales. The active, high-resolution soft matter community has made significant strides in understanding polymer dynamics, proteins, and phospholipid membranes, all with the help of this unique instrument. Pushing its capabilities to its extremes allowed to perform demanding grazing incidence experiments and were at the heart of science driven instrumentation, which leads often innovation in neutron scattering. Motion on length scales of nanometers and nanoseconds up to some 100s of nanoseconds will be the NSE domain also in the future. The unique possibility to apply contrast variation in neutron scattering in particular provides a very powerful tool to look deep into details of the motion of macromolecules.

The community grew significantly over the last decade and extracted new information on more and more complex systems. Like with the interaction of toxic components of e-cigarette vapor with pulmonary surfactants, the science moves toward more complex systems and more applied research questions where effects of lipid membrane elasticity are of relevance in medical questions. The low background in terms of neutrons and magnetic field variation due to the unique magnetically shielded room, and high stability of the superconducting instrument allow for the measurement of even minute effects with long

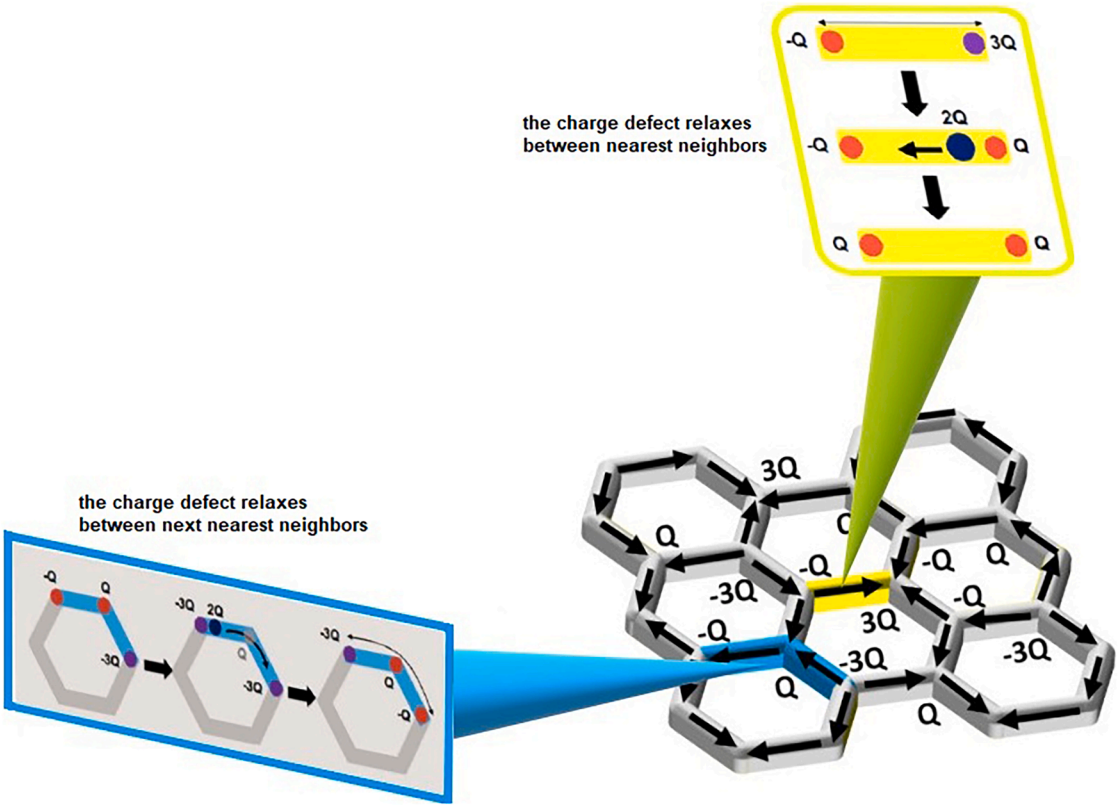

Figure 14. Magnetic charge relaxation dynamics

A honeycomb lattice schematic is shown with vertices marked by high (± 3Q) and low integer (± Q) magnetic charges where the spin relaxation processes take place. High integer charges are quasi-stable and release or absorb magnetic charge defects of 2Q unit magnitude. A magnetic charge defect traverses between nearest neighboring vertices (green elements) and between next nearest neighboring vertices (blue elements) corresponding to different reciprocal wave vectors, until it faces a high integer charge (3Q or -3Q) which serves as the roadblock. Figure based on the study by Chen et al.,[63] CC-BY-NC-ND (iScience).

measurement times. This enables the observation of phenomena such as membrane elasticity modifications, which could have a profound effect on their biological function. The user community can continue to rely on the SNS-NSE instrument for future research into details of dynamics of soft matter and biology.

Similarly, the hard matter community has also made substantial progress. After several successful initial paramagnetic measurements, the magnetism research community is pushing the boundaries further by developing a new setup for SNS-NSE experiments on quantum materials, including magnetic topological insulators and quantum spin liquids. These experiments aim to explore quasi-elastic critical scattering, vison gaps, and bound states in Kitaev quantum spin liquids, focusing on energy scales that are beyond the reach of conventional scattering techniques. This will include the development of a sub-Kelvin, ferromagnetic spin-echo setup, which will soon be available to the condensed matter community for ferromagnetism studies. This innovative setup will enable spin-echo measurements in the GHz frequency regime, an area where very few techniques exist, and none can provide reliable Q-dependent information like spin-echo.

As the sole high-resolution spin-echo spectrometer at a pulsed source, SNS-NSE offers a flexibility that is only available there. This includes the option of selecting the Q-resolution a posteriori from a broad Q and time region captured in a single setting due to the wavelength variation during the pulse. The transition to a new instrument control and data acquisition system based on EPICS, the standard at the SNS, has been completed, as has an upgrade of selected electronic components. These upgrades will enable the provision of high-resolution neutron spectroscopy at the highest possible level for the next several decades. With the SNS accelerator upgrades and the increasing power (projected to 2.0 MW), the usable Fourier time range, strongly coupled to the available neutron intensity at the beamline, will also likely increase. But it will stay in the range currently available at the instrument. Fourier times of many 100's of nanoseconds will remain difficult (or time consuming) to achieve and will be only available for special cases.

The SNS-NSE contributed actively to the advance of high-resolution spectroscopy, an area of science which is highly relevant in many areas of science. With its design the instrument can fulfill the requests of many different communities, from the extension of the classical static structure measured with small angle neutron scattering to very local effects in glass physics. The area of nanosecond dynamics on nanometer length scales is

hardly accessible with any other technique, and with the flexibility of highlighting different parts of complex multicomponent systems by contrast variation, also NSE will provide invaluable information to new challenges at the border of fundamental and applied research.

In which direction is the field of scientific research with its high-resolution capabilities evolving? From our perspective, the main area remains soft matter and biology, where the compelling questions are related not only to the role of dynamics and flexibility in membrane-protein interactions, enzymatic processes, biological membrane stability, and manipulation by elasticity changes but also to interface stability in cosmetics, food emulsions, and food related interfaces. Especially in view of sustainability in food production, the replacement of the well-established stabilized interfaces optimized by nature, for example in dairy products, with plant based alternatives, requires not only structural knowledge but also in view of rheology and elasticity. Complex liquids with multi component systems, where the separation of the self- and distinct part of the correlation function can reveal fundamental details of the liquid, as has been pushed for small molecules and short times,[66] can be extended also to more complex large-molecule liquids. In many cases, the standard ways of data interpretation reaches its limits and new paths would be desirable to pursue. In this context, we see a huge potential in the connection of NSE with molecular dynamics simulations, both techniques can provide the correlation function of a system (either in reciprocal or in real space) and allow in this respect to validate MD simulations which allow then to go further into details concerning single components or functional groups of the sample. The limiting factor so far is the required timescale of several 100's of ns in many cases for large molecules or structures such as complex interfaces, requiring a huge amount of computing power. The development of supercomputers closes this gap and potentially allows for a new paradigm in experimental workflow integrating MD as an integral part of the daily work. Data interpretation and modeling may be the area where new developments will act as a game changer in investigations of increasingly more complex systems. From the experimental side, the challenging factor will be the provision of rather large amounts of high-quality samples (in terms of monodispersity for example, or purity of the components), which is especially difficult for proteins and even more for partly deuterated biological molecules. NSE also can provide environment for high-precision measurements in nuclear physics, such as measurements of neutron incoherent scattering lengths,[67,68] which can provide valuable and missing information for specific nuclei and isotopes.

The main challenge for the community is to have access to the NSE instruments worldwide. In this respect, the SNS-NSE will provide its share for the next decades to keep these length and timescales accessible.

DECLARATION OF INTERESTS

The authors declare no competing interests.

ACKNOWLEDGMENTS

The authors would like acknowledge contributions of numerous colleagues from Forschungszentrum Jülich and Oak Ridge National Lab. In particular we extend our sincere thanks to Prof. Dieter Richter for his vision and leadership, which were instrumental in the development and construction of the SNS-NSE spectrometer. We also would like to recognize all former and current instrument scientists and staff, including Michael Ohl, Nikolas Arend, Melissa Sharp, Tadeusz Kozielewski, Malcolm Cochran, and Mary Odom.

This manuscript has been authored by UT-Battelle LLC under contract no. DE-AC05-00OR22725 with the US Department of Energy (DOE). The US government retains and the publisher, by accepting the article for publication, acknowledges that the US government retains a nonexclusive, paid-up, irrevocable, worldwide license to publish or reproduce the published form of this manuscript, or allow others to do so, for US government purposes. DOE will provide public access to these results of federally sponsored research in accordance with the DOE Public Access Plan (http://energy.gov/downloads/doe-public-access-plan).

This research used resources at the Spallation Neutron Source, a DOE Office of Science User Facility operated by the Oak Ridge National Laboratory.

AUTHOR CONTRIBUTIONS

All authors contributed equally.

REFERENCES

1. Monkenbusch, M., and Richter, D. (2007). High resolution neutron spectroscopy—a tool for the investigation of dynamics of polymers and soft matter. C. R. Phys. *8*, 845–864.
2. Mezei, F. (1972). Neutron spin echo: A new concept in polarized thermal neutron techniques. Z. Phys. *255*, 146–160.
3. F. Mezei, ed. (1980). Neutron Spin Echo vol. 128 of *Lecture Notes in Physics* (Berlin, Heidelberg, New York: Springer).
4. Sharma, V.K., Nagao, M., Rai, D.K., and Mamontov, E. (2019). Membrane softening by nonsteroidal anti-inflammatory drugs investigated by neutron spin echo. Phys. Chem. Chem. Phys. *21*, 20211–20218.
5. Smolin, N., Biehl, R., Kneller, G.R., Richter, D., and Smith, J.C. (2012). Functional domain motions in proteins on the 1–100 ns timescale: comparison of neutron spin-echo spectroscopy of phosphoglycerate kinase with molecular-dynamics simulation. Biophys. J. *102*, 1108–1117.
6. Longeville, S., and Stingaciu, L.-R. (2017). Hemoglobin diffusion and the dynamics of oxygen capture by red blood cells. Sci. Rep. *7*, 10448. https://doi.org/10.1038/s41598-017-09146-9.
7. Ehlers, G. (2006). Study of slow dynamic processes in magnetic systems by neutron spin-echo spectroscopy. J. Phys. Condens. Matter *18*, R231–R244.
8. Pappas, C., Bannenberg, L.J., Lelièvre-Berna, E., Qian, F., Dewhurst, C. D., Dalgliesh, R.M., Schlagel, D.L., Lograsso, T.A., and Falus, P. (2017). Magnetic fluctuations, precursor phenomena, and phase transition in mnsi under a magnetic field. Phys. Rev. Lett. *119*, 047203.
9. Ohl, M., Monkenbusch, M., Arend, N., Kozielewski, T., Vehres, G., Tiemann, C., Butzek, M., Soltner, H., Giesen, U., Achten, R., et al. (2012). The spin-echo spectrometer at the spallation neutron source (sns). Nucl. Instrum. Methods Phys. Res. Sect. A Accel. Spectrom. Detect. Assoc. Equip. *696*, 85–99. https://doi.org/10.1016/j.nima.2012.08.059.
10. SNS-NSE instrument website. https://neutrons.ornl.gov/nse.
11. Pasini, S., Holderer, O., Kozielewski, T., Richter, D., and Monkenbusch, M. (2019). J-nse-phoenix, a neutron spin-echo spectrometer with optimized superconducting precession coils at the mlz in garching. Rev. Sci. Instrum. *90*, 043107.
12. Mezei, F. (1979). The application of neutron spin echo on pulsed neutron sources. Nucl. Instrum. Methods *164*, 153–156. https://doi.org/10.1016/0029-554X(79)90444-0.
13. Farago, B. (2002). Time-of-flight neutron spin echo: present status. In Neutron Spin Echo Spectroscopy: Basics, Trends and Applications, F. Mezei, C. Pappas, and G. T, eds. (Berlin, Heidelberg, New York: Springer), pp. 15–34.

14. Komura, S., Takeda, T., Miyazaki, T., Saga, M., and Ueno, S. (1988). A neutron spin echo spectrometer using superconducting magnets. Nucl. Instrum. Methods Phys. Res. Sect. A Accel. Spectrom. Detect. Assoc. Equip. *267*, 425–435.

15. Rosov, N., Rathgeber, S., and Monkenbusch, M. (1999). Neutron Spin Echo Spectroscopy at the NIST Center for Neutron Research chap. ACS Symp. Ser. Am. Chem. Soc. *7*, 103–116. https://doi.org/10.1021/bk-2000-0739.ch007.

16. Zolnierczuk, P.A., Holderer, O., Pasini, S., Kozielewski, T., Stingaciu, L.R., and Monkenbusch, M. (2019). Efficient data extraction from neutron time-of-flight spin-echo raw data. J. Appl. Crystallogr. *52*, 1022–1034. https://doi.org/10.1107/S1600576719010847.

17. Marshall, W., and Lovesey, S. W. (1971). Theory of thermal neutron scattering: the use of neutrons for the investigation of condensed matter. In International series of monographs on physics (Clarendon Press).

18. Van Hove, L. (1954). Correlations in space and time and born approximation scattering in systems of interacting particles. Phys. Rev. *95*, 249–262. https://doi.org/10.1103/PhysRev.95.249.

19. Squires, G.L. (2012). Introduction to the Theory of Thermal Neutron Scattering, 3 ed. (Cambridge University Press).

20. Lipfert, F., Holderer, O., Frielinghaus, H., Appavou, M.-S., Do, C., Ohl, M., and Richter, D. (2015). Long wavelength undulations dominate dynamics in large surfactant membrane patches. Nanoscale *7*, 2578–2586. https://doi.org/10.1039/c4nr06278g.

21. Walter, W., Boffo, C., Borlein, M., Kozielewski, T., Monkenbusch, M., Ohl, M., Paul, A., Schrauth, B., Sikler, G., and Tiemann, C. (2009). Design, manufacturing and performance of a pair of superconducting solenoids for a neutron spin-echo spectrometer at the SNS. IEEE Trans. Appl. Supercond. *19*, 1320–1323, Record converted from VDB: 12.11.2012. https://doi.org/10.1109/TASC.2009.2018782.

22. Soltner, H., Pabst, U., Butzek, M., Ohl, M., Kozielewski, T., Monkenbusch, M., Sokol, D., Maltin, L., Lindgren, E., Koch, S., and Fugate, D. (2011). Design, construction, and performance of a magnetically shielded room for a neutron spin echo spectrometer. Nucl. Instrum. Methods Phys. Res. Sect. A Accel. Spectrom. Detect. Assoc. Equip. *644*, 40–47. https://doi.org/10.1016/j.nima.2011.01.094.

23. Farago, B., Falus, P., Hoffmann, I., Gradzielski, M., Thomas, F., and Gomez, C. (2015). The in15 upgrade. Neutron News *26*, 15–17.

24. Doi, M., and Edwards, S. (1994). The Theory of Polymer Dynamics Vol. 73 of *International Series of Monographs on Physics* (Oxford: Oxford University Press).

25. Richter, D., Monkenbusch, M., Arbe, A., and Colmenero, J. (2005). Neutron spin echo in polymer systems. Adv. Polym. Sci. *174*, 1–221.

26. Stingaciu, L.R., Ivanova, O., Ohl, M., Biehl, R., and Richter, D. (2016). Fast antibody fragment motion: flexible linkers act as entropic spring. Sci. Rep. *6*, 22148. https://doi.org/10.1038/srep22148.

27. Zilman, A., and Granek, R. (1996). Undulations and dynamic structure factor of membranes. Phys. Rev. Lett. *77*, 4788–4791.

28. Dykeman-Bermingham, P.A., Stingaciu, L.R., Do, C., and Knight, A.S. (2024). Dynamic implications of noncovalent interactions in amphiphilic single-chain polymer nanoparticles. ACS Macro Lett. *13*, 889–895.

29. Witte, J., Kyrey, T., Lutzki, J., Dahl, A.M., Houston, J., Radulescu, A., Pipich, V., Stingaciu, L., Kühnhammer, M., Witt, M.U., et al. (2019). A comparison of the network structure and inner dynamics of homogeneously and heterogeneously crosslinked pnipam microgels with high crosslinker content. Soft Matter *15*, 1053–1064. https://doi.org/10.1039/c8sm02141d.

30. Pasini, S., Maccarrone, S., Székely, N., Stingaciu, L., Gelissen, A., Richtering, W., Monkenbusch, M., and Holderer, O. (2020). Fluctuation suppression in microgels by polymer electrolytes. Structural Dynamics *7*, 034302.

31. Raftopoulos, K.N., Kyriakos, K., Nuber, M., Niebuur, B.-J., Holderer, O., Ohl, M., Ivanova, O., Pasini, S., and Papadakis, C.M. (2020). Co-nonsolvency in concentrated aqueous solutions of pnipam: effect of methanol on the collective and the chain dynamics. Soft Matter *16*, 8462–8472.

32. Hiroi, T., Ohl, M., Sakai, T., and Shibayama, M. (2014). Multiscale dynamics of inhomogeneity-free polymer gels. Macromolecules *47*, 763–770. https://doi.org/10.1021/ma402439v.

33. Shibayama, M., Nishi, K., and Hiroi, T. (2015). Gelation kinetics and polymer network dynamics of homogeneous tetra-peg gels. Macromol. Symp. *348*, 9–13. Wiley Online Library.

34. Wijesinghe, S., Kosgallana, C., Senanayake, M., Mohottalalage, S.S., Zolnierczuk, P., Stingaciu, L., Grest, G.S., and Perahia, D. (2024). From ionic clusters dynamics to network constraints in ionic polymer solutions. Phys. Rev. E *109*, 034501.

35. Kosgallana, C., Wijesinghe, S., Senanayake, M., Mohottalalage, S.S., Ohl, M., Zolnierczuk, P., Grest, G.S., and Perahia, D. (2024). From molecular constraints to macroscopic dynamics in associative networks formed by ionizable polymers: A neutron spin echo and molecular dynamics simulations study. ACS Polym. Au *4*, 149–156.

36. Krutyeva, M., Wischnewski, A., Monkenbusch, M., Willner, L., Maiz, J., Mijangos, C., Arbe, A., Colmenero, J., Radulescu, A., Holderer, O., et al. (2013). Effect of nanoconfinement on polymer dynamics: Surface layers and interphases. Phys. Rev. Lett. *110*, 108303–108305.

37. Kim, S.Y., Meyer, H.W., Saalwächter, K., and Zukoski, C.F. (2012). Polymer dynamics in peg-silica nanocomposites: Effects of polymer molecular weight, temperature and solvent dilution. Macromolecules *45*, 4225–4237.

38. Goswami, M., Iyiola, O.O., Lu, W., Hong, K., Zolnierczuk, P., Stingaciu, L.-R., Heller, W.T., Taleb, O., Sumpter, B.G., and Hallinan, D.T. (2023). Understanding interfacial block copolymer structure and dynamics. Macromolecules *56*, 762–771.

39. Krutyeva, M., Pasini, S., Monkenbusch, M., Allgaier, J., Maiz, J., Mijangos, C., Hartmann-Azanza, B., Steinhart, M., Jalarvo, N., Ivanova, O., et al. (2017). Polymer dynamics under cylindrical confinement featuring a locally repulsive surface: A quasielastic neutron scattering study. J. Chem. Phys. *146*, 203306. https://doi.org/10.1063/1.4979809.

40. Jaksch, S., Holderer, O., Gvaramia, M., Ohl, M., Monkenbusch, M., and Frielinghaus, H. (2017). Nanoscale rheology at solid-complex fluid interfaces. Sci. Rep. *7*, 4417. https://doi.org/10.1038/s41598-017-04294-4.

41. Jaksch, S., Holderer, O., Frielinghaus, H., Koutsioubas, A., Zolnierczuk, P., Hayward, D.W., Förster, S., and Müller-Buschbaum, P. (2021). Influence of nacl on the structure and dynamics of phospholipid layers. Front. Physiol. *9*, 628219. https://doi.org/10.3389/fphy.2021.628219.

42. Frielinghaus, H., Dubey, P.S., Wu, B., Odom, M., Zheng, F., Shin, E., Zolnierczuk, P., Holderer, O., Förster, S., and Heiden-Hecht, T. (2023). Experimental critical dynamics of 3-methyl pyridine/d2o mixtures without and with antagonistic salt. Phys. Rev. Res. *5*, 023053.

43. Frielinghaus, H., Holderer, O., Lipfert, F., Monkenbusch, M., Arend, N., and Richter, D. (2012). Scattering depth correction of evanescent waves in inelastic neutron scattering using a neutron prism. Nucl. Instrum. Methods Phys. Res. Sect. A Accel. Spectrom. Detect. Assoc. Equip. *686*, 71–74. https://doi.org/10.1016/j.nima.2012.05.064.

44. Frielinghaus, H., Gvaramia, M., Mangiapia, G., Jaksch, S., Ganeva, M., Koutsioubas, A., Mattauch, S., Ohl, M., Monkenbusch, M., and Holderer, O. (2017). New tools for grazing incidence neutron scattering experiments open perspectives to study nano-scale tribology mechanisms. Nucl. Instrum. Methods Phys. Res. Sect. A Accel. Spectrom. Detect. Assoc. Equip. *871*, 72–76.

45. Frielinghaus, H., Kerscher, M., Holderer, O., Monkenbusch, M., and Richter, D. (2012). Acceleration of membrane dynamics adjacent to a wall. Phys. Rev. *85*, 041408.

46. Lipfert, F., Frielinghaus, H., Holderer, O., Mattauch, S., Monkenbusch, M., Arend, N., and Richter, D. (2014). Polymer enrichment decelerates surfactant membranes near interfaces. Phys. Rev. *89*, 042303. https://doi.org/10.1103/PhysRevE.89.042303.

47. Hayward, D.W., Jaksch, S., Fomina, M., Dubey, P.S., Frielinghaus, H., Holderer, O., and Monkenbusch, M. (2022). Membranedyn: simulating the dynamics of supported membrane stacks on the nanosecond timescale. Acta Crystallogr. D Struct. Biol. *78*, 1249–1258.

48. Romanov, V.P., and Ul'yanov, S.V. (2002). Dynamic and correlation properties of solid supported smectic- A films. Phys. Rev. *66*, 061701. https://doi.org/10.1103/PhysRevE.66.061701.

49. Khatri, B.S., and McLeish, T.C.B. (2007). Rouse model with internal friction: a coarse grained framework for single biopolymer dynamics. Macromolecules *40*, 6770–6777. https://doi.org/10.1021/ma071175x.

50. Cheng, R.R., Hawk, A.T., and Makarov, D.E. (2013). Exploring the role of internal friction in the dynamics of unfolded proteins using simple polymer models. J. Chem. Phys. *138*, 074112.

51. Balacescu, L., Schrader, T.E., Radulescu, A., Zolnierczuk, P., Holderer, O., Pasini, S., Fitter, J., and Stadler, A.M. (2020). Transition between protein-like and polymer-like dynamic behavior: Internal friction in unfolded apomyoglobin depends on denaturing conditions. Sci. Rep. *10*, 1570. https://doi.org/10.1038/s41598-020-57775-4.

52. Chakraborty, S., Doktorova, M., Molugu, T.R., Heberle, F.A., Scott, H.L., Dzikovski, B., Nagao, M., Stingaciu, L.-R., Standaert, R.F., Barrera, F.N., et al. (2020). How cholesterol stiffens unsaturated lipid membranes. USA *117*, 21896–21905. https://doi.org/10.1073/pnas.2004807117.

53. Krugmann, B., Radulescu, A., Appavou, M.-S., Koutsioubas, A., Stingaciu, L.R., Dulle, M., Förster, S., and Stadler, A.M. (2020). Membrane stiffness and myelin basic protein binding strength as molecular origin of multiple sclerosis. Sci. Rep. *10*, 16691. https://doi.org/10.1038/s41598-020-73671-3.

54. Dziura, M., Castillo, S.R., DiPasquale, M., Gbadamosi, O., Zolnierczuk, P., Nagao, M., Kelley, E.G., and Marquardt, D. (2023). Investigating the effect of medium chain triglycerides on the elasticity of pulmonary surfactant. Chem. Res. Toxicol. *36*, 643–652. https://doi.org/10.1021/acs.chemrestox.2c00349.

55. Heller, W.T., and Zolnierczuk, P.A. (2019). The helix-to-sheet transition of an hiv-1 fusion peptide derivative changes the mechanical properties of lipid bilayer membranes. Biochim. Biophys. Acta Biomembr. *1861*, 565–572. https://doi.org/10.1016/j.bbamem.2018.12.004.

56. Scott, H.L., Burns-Casamayor, V., Dixson, A.C., Standaert, R.F., Stanley, C.B., Stingaciu, L.-R., Carrillo, J.-M.Y., Sumpter, B.G., Katsaras, J., Qiang, W., et al. (2024). Neutron spin echo shows phlip is capable of retarding membrane thickness fluctuations. Biochim. Biophys. Acta Biomembr. *1866*, 184349.

57. De Mel, J.U., Gupta, S., Perera, R.M., Ngo, L., Zolnierczuk, P., Bleuel, M., Pingali, S.V., and Schneider, G.J. (2020). Influence of external nacl salt on membrane rigidity of neutral dopc vesicles. Langmuir *36*, 9356–9367. https://doi.org/10.1021/acs.langmuir.0c01004.

58. De Mel, J.U., Gupta, S., Willner, L., Allgaier, J., Stingaciu, L.R., Bleuel, M., and Schneider, G.J. (2021). Manipulating phospholipid vesicles at the nanoscale: A transformation from unilamellar to multilamellar by an n-alkyl-poly(ethylene oxide). Langmuir *37*, 2362–2375. https://doi.org/10.1021/acs.langmuir.0c03302.

59. Nickels, J.D., Cheng, X., Mostofian, B., Stanley, C., Lindner, B., Heberle, F.A., Perticaroli, S., Feygenson, M., Egami, T., Standaert, R.F., et al. (2015). Mechanical properties of nanoscopic lipid domains. J. Am. Chem. Soc. *137*, 15772–15780.

60. Qian, S., and Zolnierczuk, P.A. (2022). Interaction of a short antimicrobial peptide on charged lipid bilayer: A case study on aurein 1.2 peptide. BBA Adv. *2*, 100045.

61. Stingaciu, L.R., O'Neill, H., Liberton, M., Urban, V.S., Pakrasi, H.B., and Ohl, M. (2016). Revealing the dynamics of thylakoid membranes in living cyanobacterial cells. Sci. Rep. *6*, 19627.

62. Stingaciu, L.R., O'Neill, H., Liberton, M., Pakrasi, H.B., and Urban, V.S. (2019). Influence of chemically disrupted photosynthesis on cyanobacterial thylakoid dynamics in synechocystis sp. pcc 6803. Sci. Rep. *9*, 1–9.

63. Chen, Y., Yumnam, G., Guo, J., Stingaciu, L., Zolnierczuk, P., Lauter, V., and Singh, D.K. (2021). Magnetic charge's relaxation propelled electricity in two-dimensional magnetic honeycomb lattice. iScience *24*, 102206.

64. Guo, J., Ghosh, P., Hill, D., Chen, Y., Stingaciu, L., Zolnierczuk, P., Ullrich, C.A., and Singh, D.K. (2023). Persistent dynamic magnetic state in artificial honeycomb spin ice. Nat. Commun. *14*, 5212.

65. Guo, J., Hill, D., Lauter, V., Stingaciu, L., Zolnierczuk, P., Ullrich, C.A., and Singh, D.K. (2024). Emergent topological quasiparticle kinetics in constricted nanomagnets. Phys. Rev. Res. *6*, 043144.

66. Arbe, A., Nilsen, G.J., Stewart, J.R., Alvarez, F., Sakai, V.G., and Colmenero, J. (2020). Coherent structural relaxation of water from meso-to intermolecular scales measured using neutron spectroscopy with polarization analysis. Phys. Rev. Res. *2*, 022015.

67. Lu, H., Holderer, O., Ioffe, A., Pasini, S., Pistel, P., Salhi, Z., Goodson, B. M., Snow, W.M., and Babcock, E. (2023). Precise approach to determining the he 3 neutron incoherent scattering length bi. Phys. Rev. C *108*, L031001.

68. Lu, H., Barlow, M.J., Basler, D., Gutfreund, P., Holderer, O., Ioffe, A., Pasini, S., Pistel, P., Salhi, Z., Zhernenkov, K., et al. (2024). First measurement of neutron birefringence in polarized xe 129 and xe 131 nuclei. Phys. Rev. C *109*, L011001.

69. Holderer, O. (2019). Dynamics of Large Molecules and Membranes Chap. B4 (Jülich: Forschungszentrum Jülich Schriften des Forschungszentrums Jülich Reihe Schlüsseltechnologien), pp. 1–15.